

X-ray detection by direct modulation of losses in a laser cavity

Cite as: Appl. Phys. Lett. 117, 234101 (2020); <https://doi.org/10.1063/5.0029002>

Submitted: 08 September 2020 . Accepted: 20 November 2020 . Published Online: 08 December 2020

 F. Chioffi,  C. Braggio, M. Aresti, G. Carugno,  F. Quochi,  A. Lai,  F. Pirzio, and  S. Vasiukov



View Online



Export Citation




CrossMark



Measure Ready
MCS-EMP Modular Characterization Systems

NEW Multi-purpose platforms for automated variable-field experiments





Find out more

X-ray detection by direct modulation of losses in a laser cavity

Cite as: Appl. Phys. Lett. **117**, 234101 (2020); doi: [10.1063/5.0029002](https://doi.org/10.1063/5.0029002)

Submitted: 8 September 2020 · Accepted: 20 November 2020 ·

Published Online: 8 December 2020



View Online



Export Citation



CrossMark

F. Chiossi,^{1,2}  C. Braggio,^{1,2,a)}  M. Aresti,³ C. Carugno,^{1,2} F. Quochi,^{3,4}  A. Lai,³  F. Pirzio,⁵  and S. Vasiukov² 

AFFILIATIONS

¹Dipartimento di Fisica e Astronomia, Università di Padova, via F. Marzolo 8, 35131 Padova, Italy

²INFN, Sezione di Padova, via F. Marzolo 8, 35131 Padova, Italy

³INFN, Sezione di Cagliari, Complesso Universitario di Monserrato, I-09042 Monserrato (Cagliari), Italy

⁴Dipartimento di Fisica, Università di Cagliari, Complesso Universitario di Monserrato, I-09042 Monserrato (Cagliari), Italy

⁵Dipartimento di Ingegneria Industriale e dell'Informazione, Università di Pavia, via Ferrata 5, 27100 Pavia, Italy

^{a)} Author to whom correspondence should be addressed: caterina.braggio@unipd.it

ABSTRACT

In this work, we experimentally explore the possibility to realize a sensor whose basic building block is a laser cavity that hosts a target crystal for the incident ionizing radiation. Two possible detection mechanisms are considered: a process of coherent scintillation related to the rapid decay via stimulated emission of the excited atomic or molecular levels of the target material and the activation of states that absorb intracavity photons. We use a solid-state laser to study the dynamic response of our prototype sensor and the related intrinsic limitations and demonstrate capability to detect x-ray energy down to 10 GeV.

© 2020 Author(s). All article content, except where otherwise noted, is licensed under a Creative Commons Attribution (CC BY) license (<http://creativecommons.org/licenses/by/4.0/>). <https://doi.org/10.1063/5.0029002>

One of the processes that are mostly exploited in radiation detection is scintillation, whereby light in transparent media is emitted following the absorption of ionizing radiation. Scintillation is the result of spontaneous decay, with a relatively slow fluorescence decay time and isotropic emission.¹ To overcome this intrinsic limitation, the authors have recently proposed methods of radiation detection based on the modulation of optical properties. For instance, refractive index n modulation in a cadmium telluride (CdTe) crystal has been used to obtain a modulation signal with a radionuclide source (Ge-68) as the source of ionization.² Using the same physical principle, i.e., the n -index modulation induced by radiation interaction in semiconductors, ultrafast x-ray detection for imaging applications at ignition facilities has also been accomplished using a Mach-Zehnder interferometer as a readout device.^{3,4}

The present work adds to these alternative approaches in radiation detection, introducing a promising mechanism that might be exploited to obtain faster timing and higher sensitivity in medical imaging applications. To get time of flight (TOF) information in positron emission tomography (PET), would lead to a much improved SNR if sub-100 ps resolution is accomplished.¹ Fast timing and high sensitivity are also required for dosimeters in radiotherapy, in which

the dose delivered during the treatment could be more efficiently monitored.^{5,6}

The concept we rely on is schematized in Fig. 1, where an optical laser cavity between the end mirror (EM) and the output coupler (OC) displays an interaction region for the ionizing radiation, besides its active crystal in which population inversion is accomplished with an external pump laser. Ionizing radiation, absorbed within the material volume traversed by the optical cavity mode, can give rise to excitation of atomic levels of the target crystal that decay via rapid emission of coherent scintillation light or activation of states that absorb at the cavity wavelength.

Hereafter, we will refer to the first as *gain switching*, a technique used to generate ps-duration pulses via electrons injection in the active region of semiconductor lasers,⁷ while the second is the loss modulation approach.

Our motivating questions for this work are: Can we detect laser output changes from the interaction of radiation in the target crystal? Can fast timing or high temporal resolution be accomplished by exploiting the stimulated emission or absorption within a laser cavity?

To address these points, we built a prototype laser cavity and conducted optical tests with a LED source to infer the quantum

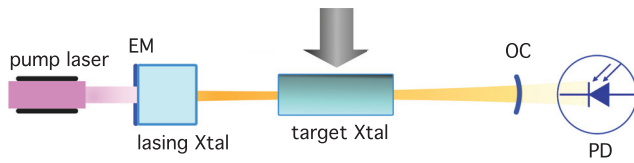


FIG. 1. Schematic representation of the present method for radiation detection based on an optical laser cavity between EM (end mirror) and OC (output coupler) mirrors. Ionizing radiation interacts in a region optically connected to the laser cavity mode in the target crystal and is detected by variations of the laser output intensity. The gray arrow represents the incident radiation originating from an optical, gamma, or x-ray source.

efficiency of our detector and to understand the factors that determine the response time in gain switching. Using an x-ray source, we tested the loss modulation approach and measured the related x-ray energy threshold.

The laser we developed to conduct the optical and x-ray tests is a diode-pumped solid state laser. The collimated output of a fiber-coupled laser diode tuned at ~ 808 nm is focused on the a-cut, 2 mm-long, 2%-doped Nd:YVO₄ laser active crystal. The end mirror of the cavity is the coated input face of the Nd:YVO₄ crystal (highly reflective dielectric coating at 1064 nm and high transmissivity at 808 nm), whereas a concave mirror with a radius of curvature of 30 cm is the laser output coupler. When inserted in the cavity, the target crystal introduces additional losses, as shown in the output power vs input power plot in Fig. 2. In this case, the target crystal is an a-cut, 5 mm-long, 1%-doped Nd:YVO₄.

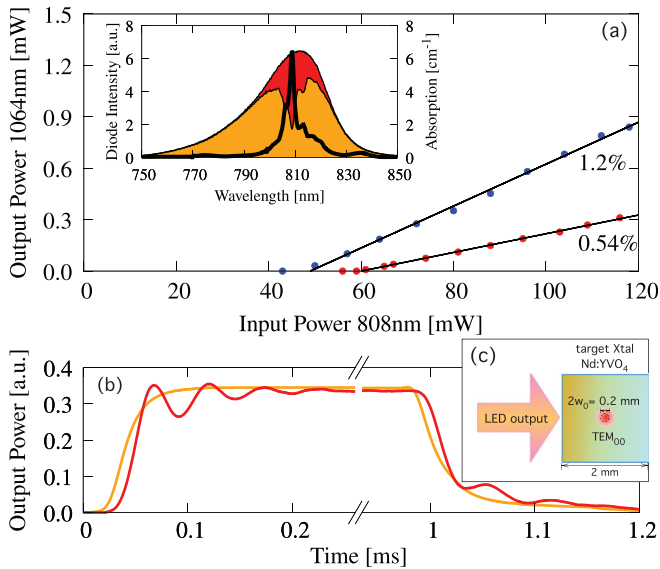


FIG. 2. (a) Output power vs pump laser input power with (red dots) and without (blue dots) the target crystal. In the inset, the Nd:YVO₄ absorption spectrum (black line) is superimposed on the diode emission (red+orange area) and transmission (orange area) spectrum, which are used to calculate the fraction of energy released within the active detector volume. (b) LED excitation pulse and corresponding laser output response are shown as orange and red lines, respectively. Relaxation oscillations are observed in the laser output. (c) Side-pumping geometry used for excitation of the target crystal.

To maximize sensitivity, the laser cavity should host the minimum number of intracavity photons. We, thus, operate it at the lasing threshold during both the optical and x-ray tests, where relatively large intensity fluctuations are observed. As the cavity is not stabilized by any feedback electronics, it exhibits long-term drifts from 200 nW to few μ W output power.

Under these conditions, we investigated the positive gain concept by injecting in the target crystal the light signal depicted in Fig. 2. The light signal is generated by driving the current of an LED source with a few hundred microseconds duration square electronic pulses. The LED output spectrum is centered at the maximum of the absorption in Nd:YVO₄, corresponding to the transition from the ground state $^4I_{9/2}$ to the $^4F_{5/2}$ manifold. The LED photons absorbed within the active detector volume, i.e., within the crystal region crossed by the laser TEM₀₀ mode, are calculated through the ratio between the integrals of the Nd:YVO₄ absorption spectrum and the emission spectrum of the LED shown in the inset of Fig. 2(a). Note that in these measurements, the laser mode, whose waist is 100 μ m, is centered on the target crystal and the optical beam travels in the target crystal approximately 900 μ m before reaching the sensitive region.

We calculate the detector quantum efficiency as the ratio between the number of photons emitted by the laser cavity at 1064 nm and the number of input LED photons absorbed in the active volume. The same efficiency value is obtained for several injected LED powers from a few tens to thousands W/cm².

As shown in Fig. 2(b), where the temporal response of the detector is shown, recorded at the output of an InGaAs photodiode, we identify damped relaxation oscillations at ~ 100 kHz as the well-known transient response of an oscillator to an external driving force.⁸ For small oscillations about the steady state values, a linearized analysis gives analytical solutions for the damping rate and relaxation oscillation frequency ω_r . The latter is usually given by the geometric mean of the atomic relaxation time τ_2 and the cavity field recovery time τ_c as $\omega_r = \sqrt{\frac{x-1}{\tau_c \tau_2}}$, with x amount by which pumping threshold is exceeded. In our crystal, $\tau_2 = 90$ μ s and the observed ringing period is about 50 μ s. The related detector response time cannot be faster than a fraction of this period. Even though it can be substantially reduced by choosing materials with much shorter τ_2 ,⁹ this slow response might significantly limit the applicability of gain switching to TOF-PET, also in the case of much shorter cavities (i.e., smaller τ_c).

Alternatively, by modulating the losses of a laser cavity operating slightly above the threshold, the temporal response is independent of the excited level lifetime, and it is governed only by τ_c .⁸ Since, in practical cases, τ_c is of the order of few cavity round trip time, the response time of the detector can, in principle, be reduced to tens of ps by a proper design of the laser resonator. The underlying transient loss mechanism that triggers the switch-off of the laser could be directly related to electron or hole trap states that absorb photons at the laser wavelength.

These states can be generated by exciting the material using UV radiation¹⁰ or by x-rays.¹¹ In the following, we will focus on the second excitation source, with the aim of establishing an energy detection threshold E_0 for our prototype detector. This is accomplished through a measurement of the minimum energy that must be deposited in the target crystal to observe laser output changes. In particular, such a

measurement provides the value of x-ray pulse energy required to switch off the laser emission, as portrayed in Fig. 6.

We use x-ray pulses produced by a battery-operated, high-energy (75 kV) pulsed electron gun.¹² X-rays are generated by bremsstrahlung in a 10 μm-thick tantalum target. To determine the threshold E_0 of our prototype detector, both the energy and the spectrum of the x ray pulse must be carefully measured, as the stopping power depends on the photon energy as displayed in Fig. 3 for the target crystal.¹³ In the figure, we also report the x-ray spectrum we recorded using a Ge detector, together with the ²⁴¹Am source spectrum used for calibration.

Concerning the measurement of the pulse energy, we adopt the strategy represented in Fig. 4 and detailed in the following. As the Tantalum foil is electrically isolated, it is possible to monitor the injected electron current Q_{bs} , proportional to the x-ray beam intensity, and the conversion factor is obtained using a scintillator detector (CsI:Tl) whose light yield (LY) is known.¹⁴ In the inset of Fig. 4, we show examples of output detector signals corresponding to the current injection pulses, and in the main plot, we report the area of the scintillator pulses Q_d for an injected charge Q_{bs} up to about 50 nC. As the electron beam sweep is asymmetrical, generation of alternate x-ray pulses is obtained corresponding to different efficiencies. Thus, two different slope data trends are observed (see the main plot in Fig. 4), and in the following, we use their average values. A direct connection between Q_d and the X ray beam energy E_X is obtained through the following expression:

$$Q_d = eLY\eta E_X, \quad (1)$$

where $\eta = 0.8$ is the detector quantum efficiency. The value of $LY = 6.2 \times 10^4$ ph/MeV at the x-ray energy of a few tens of keV is used. During the measurements, we can, thus, directly relate the measured injected charge to the X ray pulse energy E_X .

Only a fraction of E_X is deposited within the active volume of the target crystal, i.e., the part of the crystal intersected by the laser field mode. A precise estimate of this fraction is obtained using the following procedure. We use the normalized x-ray energy spectrum

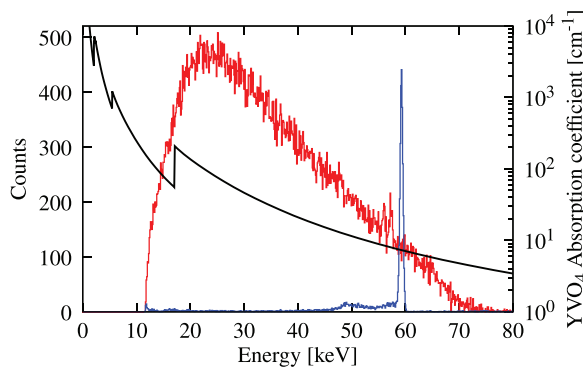


FIG. 3. Spectra of the generated x-rays (in red) and the ²⁴¹Am source used for calibration (in blue). The Ge detector (ORTEC) output signal is pre-amplified, and a shaping time of μs has been used to acquire the spectrum at a multichannel analyzer. The plot displays the YVO₄ absorption coefficient used for the calculation of the x-ray energy beam loss at different distances from the surface of the target crystal (Fig. 5).

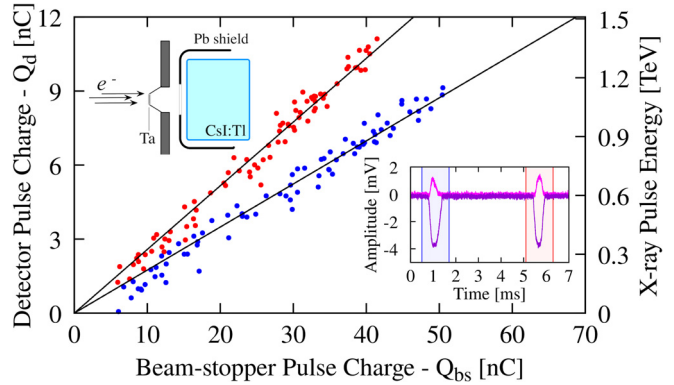


FIG. 4. X-ray pulse energy measurement: the charge of the pulse is measured using a CsI:Tl scintillator for different values of the current injection pulses Q_{bs} measured at the electron beam stopper. As the light yield of the scintillator is known, we can, thus, relate Q_d to the x-ray beam energy E_X , reported in the right vertical axis. An example of current injection signals (negative pulses) with their corresponding scintillation light outputs at the CsI:Tl detector is shown in the inset.

$S(E)$ to express the fraction of x-rays with energy E absorbed between crystal penetration depths x_1 and x_2 as

$$\frac{S_{ab}(E; x_1, x_2)}{S(E)} = e^{\mu(E)x_1} - e^{\mu(E)x_2}. \quad (2)$$

Thus, the total energy deposited in the region $[x_1, x_2]$, in the approximation of the point source for the x-ray production, is given by

$$E[x_1, x_2] = E_X \frac{d\Omega}{\Omega} \int S(E)[e^{\mu(E)x_1} - e^{\mu(E)x_2}]E dE, \quad (3)$$

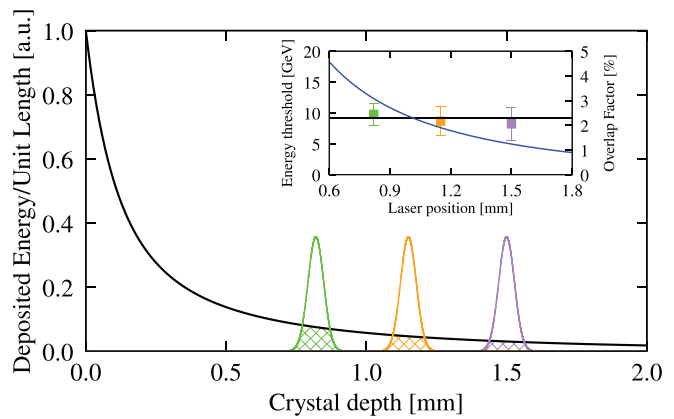


FIG. 5. Calculated x-ray beam energy released per unit length in the target crystal as a function of depth (black line). The Gaussian peaks represent the laser beam intensity profiles at positions, measured from the target crystal edge, where the detector energy threshold is estimated (inset, left scale). The average value of the latter is indicated by the black line in the inset. The fraction of the x-ray energy deposited within the crystal depth range related to the laser active volume is qualitatively described for the three laser beam positions by the evidenced areas in the main plot. The overlap factor (blue line, right scale) represents the same quantity as a function of a general laser beam position in the inset.

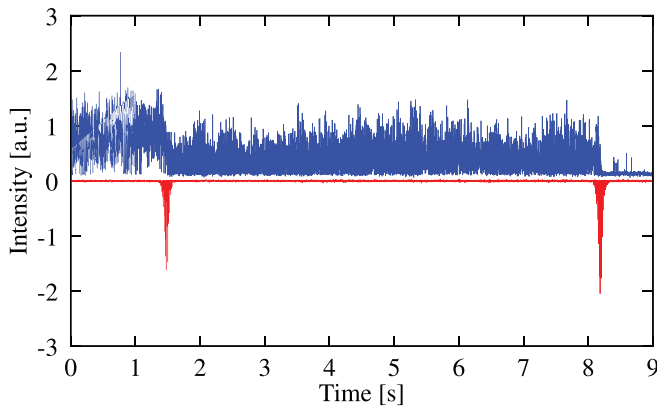


FIG. 6. The incident radiation switches the laser off. The red trace corresponds to the x-ray excitation (two different energy bunches of about 200 μ s-duration x-ray pulses), while the blue signal is the laser output at threshold detected at an InGaAs low noise photodiode. It is evident that the second pulse is sufficiently intense to switch off the laser emission.

where $\frac{d\Omega}{\Omega} = \frac{\phi L}{2\pi d^2}$ is the solid angle subtended by ϕL , transverse area of the intersection between the laser beam and the target crystal volumes.

In the main plot of Fig. 5, we report the values of the integral given by Eq. (3) for crystal depths x_1 up to 2 mm, using bin values $x_2 - x_1 = 1 \mu\text{m}$. The curve reported in the inset is instead the fraction of energy released in the active volume of the target crystal as a function of the laser beam position. We have investigated the laser output behavior for the three different positions of the optical beam, represented by the Gaussian intensity profiles. Equation (3) allows us to estimate the energy threshold of the detector once we measure the minimum x-ray pulse energy E_X^{min} required to switch off the laser output. An example of the laser output temporal response to the x-ray excitation is illustrated in Fig. 6. The calculated values for the three investigated configurations are compatible and give an average threshold value of $9 \pm 0.5 \text{ GeV}$. Our result is strengthened by the indication that the increasing values of E_X^{min} are required to perturb the laser output when the optical beam is set at greater crystal depths.

Beyond repeating the measurements with the optically active volume at different crystal depths, we validated our procedure by substituting the Nd:YVO₄ crystal with a 10%-doped Yb:KGW sample, a material in which a strong x-ray absorption is expected due to its high density (7.3 g/cm³, compared to 4.24 g/cm³ of Nd:YVO). In this case, the x-ray pulses did not alter in any way the laser output, ruling out thermal mechanisms underlying our findings.

Depending on the x-ray pulse energy and the initial intracavity laser intensity, the prototype detector may take up to several seconds to reset after the x-ray pulse, indicating the creation of long-lived, deep traps. This determines the dead time of the detector, which can be significantly shortened if excited states with shorter recombination time are exploited.

In conclusion, we have analyzed two mechanisms to detect ionizing radiation with a laser cavity. In one case, radiation incident on an intracavity target crystal contributes to the generation of photons at the laser wavelength, whereas in the second process, we

considered that it leads to the formation of excited states that switch the laser off. For experimental tests concerning the energy detection threshold, we focused on the latter, as it appears more promising for applications where a fast prompt response (sub-100 ps) is required as, for instance, in TOF-PET and hadron dosimetry.^{1,5,15}

With a prototype diode-pumped laser cavity based on Nd:YVO₄ as both a lasing medium and a target crystal, we obtained a detection threshold of 10 GeV, several orders of magnitude from the single gamma level in PET systems, yet reasonable for dosimetry applications. This result has been obtained in spite of efficiently populating the Nd ⁴F_{3/2} manifold, as proven by studies of its infrared emission in Nd:YAG.¹⁶ This mechanism is in contrast to the loss modulation approach.

A thorough study of the underlying transient absorption mechanism and further tests on different materials are necessary to improve on the present results. Candidate materials are those in which more excited states per unit deposited energy are generated with a larger absorption cross section at the laser wavelength.

This work was financially supported by the ATTRACT project funded by the EC under Grant Agreement No. 777222 and by INFN within the AXIOMA project.

DATA AVAILABILITY

The data that support the findings of this study are available from the corresponding author upon reasonable request.

REFERENCES

- C. Dujardin, E. Auffray, E. Bourret-Courchesne, P. Dorenbos, P. Lecoq, M. Nikl, A. N. Vasil'ev, A. Yoshikawa, and R. Zhu, "Needs, trends, and advances in inorganic scintillators," *IEEE Trans. Nucl. Sci.* **65**, 1977–1997 (2018).
- L. Tao, H. M. Daghighian, and C. S. Levin, "A promising new mechanism of ionizing radiation detection for positron emission tomography: Modulation of optical properties," *Phys. Med. Biol.* **61**, 7600–7622 (2016).
- K. L. Baker, R. E. Stewart, P. T. Steele, S. P. Vernon, and W. W. Hsing, "Ultrafast semiconductor x-ray detector," *Appl. Phys. Lett.* **101**, 031107 (2012).
- M. E. Lowry, C. V. Bennett, S. P. Vernon, R. Stewart, R. J. Welty, J. Heebner, O. L. Landen, and P. M. Bell, "X-ray detection by direct modulation of an optical probe beam—Radsensor: Progress on development for imaging applications," *Rev. Sci. Instrum.* **75**, 3995–3997 (2004).
- S. Avino, V. D'Avino, A. Giorgini, R. Pacelli, R. Liuzzi, L. Cella, P. De Natale, and G. Gagliardi, "Detecting ionizing radiation with optical fibers down to biomedical doses," *Appl. Phys. Lett.* **103**, 184102 (2013).
- K. Parodi, F. Ponisch, and W. Enghardt, "Experimental study on the feasibility of in-beam pet for accurate monitoring of proton therapy," *IEEE Trans. Nucl. Sci.* **52**, 778–786 (2005).
- K. Y. Lau, "Gain switching of semiconductor injection lasers," *Appl. Phys. Lett.* **52**, 257–259 (1988).
- E. Siegman, *Lasers* (University Science Books, Sausalito, CA, 1986).
- B. Wellmann, D. J. Spence, and D. W. Coutts, "Tunable continuous-wave deep-ultraviolet laser based on Ce: LiCAF," *Opt. Lett.* **39**, 1306–1309 (2014).
- H. R. Xia, X. L. Meng, M. Guo, L. Zhu, H. J. Zhang, and J. Y. Wang, "Spectral parameters of Nd-doped yttrium orthovanadate crystals," *J. Appl. Phys.* **88**, 5134–5137 (2000).
- S. Erdei, L. Kovács, Á. Pető, J. Vandlík, P. D. Townsend, and F. W. Ainger, "Low temperature three-dimensional thermoluminescence spectra of undoped YVO₄ single crystals grown by different techniques," *J. Appl. Phys.* **82**, 2567–2571 (1997).

- ¹²L. Barcellan, E. Berto, G. Carugno, G. Galet, G. Galeazzi, and A. F. Borghesani, "A battery-operated, stabilized, high-energy pulsed electron gun for the production of rare gas excimers," *Rev. Sci. Instrum.* **82**, 095103 (2011).
- ¹³"NIST standard reference database 66," <https://www.nist.gov/pml/x-ray-form-factor-attenuation-and-scattering-tables>.
- ¹⁴L. Ahle, G. Bizarri, L. Boatner, N. Cherepy, W.-S. Choong, W. Moses, S. Payne, K. Shah, S. Sheets, and B. Sturm, "Studies of non-proportionality in alkali halide and strontium iodide scintillators using SLYNCI," *MRS Proc.* 1164-L07-04 (2009).
- ¹⁵S. O'Keeffe, "Optical fibres for radiation dosimetry," in *Fiber Optic Sensors. Smart Sensors, Measurement and Instrumentation*, edited by J. Corres, I. Matias, and S. Ikezawa (Springer, Cham, 2017), Vol. 21.
- ¹⁶A. F. Borghesani, C. Braggio, G. Carugno, F. Chiossi, and M. Guarise, "Cathodo- and radioluminescence of Tm^{3+} :YAG and Nd^{3+} :YAG in an extended wavelength range," *J. Lumin.* **190**, 29–36 (2017).